

# Algorithm 1001: IPscatt—A MATLAB Toolbox for the Inverse Medium Problem in Scattering

FLORIAN BÜRCEL, University of Bremen, Center for Industrial Mathematics, Germany.

KAMIL S. KAZIMIERSKI, University of Graz, Institute of Mathematics and Scientific Computing, Austria.

ARMIN LECHLEITER, University of Bremen, Center for Industrial Mathematics, Germany.

IPscatt is a free, open-source MATLAB toolbox facilitating the solution for time-independent scattering (also known as time-harmonic scattering) in two- and three-dimensional setting. The toolbox has three main application cases: simulation of the scattered field for a given transmitter-receiver geometry; the generation of simulated data as well as the handling of the real-world data from Institute Fresnel; the reconstruction of the contrast from several measured, scattered fields. In each case a variety of options tailored to the needs of practitioners is provided. For example, the toolbox allows the simulation of the scattered near field as well as of the far field. Also, it provides methods for the modeling of the incident field as point sources as well as plane waves. Finally, many common geometries of transmitters and receivers are included out of the box. Regarding the reconstruction, the provided functions implement the regularization scheme that relies on a primal-dual algorithm and was introduced in [F. Bürgel, K. S. Kazimierski, and A. Lechleiter 2017 *Journal of Computational Physics*, 339:1–30]. This paper provides a survey of the mathematical concepts in scattering, connects them with the provided implementation, gives an overview of the software framework as well as its application areas and compares it with existing software packages solving the same problem.

CCS Concepts: • **Mathematics of computing** → **Convex optimization**; *Integral equations*; Numerical analysis; *Partial differential equations*.

Additional Key Words and Phrases: Inverse Scattering Problem, Parameter Identification, Helmholtz Equation, MATLAB Toolbox, Denoising, Sparsity Regularization, Total Variation Regularization, Primal-Dual Algorithm.

## ACM Reference Format:

Florian Bürgel, Kamil S. Kazimierski, and Armin Lechleiter. 2019. Algorithm 1001: IPscatt—A MATLAB Toolbox for the Inverse Medium Problem in Scattering. *ACM Trans. Math. Softw.* 45, 4, Article 45 (December 2019), 20 pages. <https://doi.org/10.1145/3328525>

## 1 INTRODUCTION

The mathematical model of time-independent scattering (also known as time-harmonic scattering), i.e. the electromagnetic and acoustic scattering based on the Helmholtz equation, is known in literature as the *direct scattering problem*. Fast numerical solvers for that problem are described for example in [Vainikko 2000]. The task of identifying the contrast, defined in (1), of a penetrable medium from the measurements of the waves scattered from that medium is commonly referred to as the *inverse medium problem*. In particular, this task is encountered in remote-sensing and non-destructive testing applications.

---

Authors' addresses: Florian Bürgel, [fbuergel@uni-bremen.de](mailto:fbuergel@uni-bremen.de), University of Bremen, Center for Industrial Mathematics, Germany. Kamil S. Kazimierski, [kazimier@uni-graz.at](mailto:kazimier@uni-graz.at), University of Graz, Institute of Mathematics and Scientific Computing, Austria. The Institute of Mathematics and Scientific Computing is a member of NAWI Graz ([www.nawigratz.at](http://www.nawigratz.at)) and BioTechMed Graz ([www.biotechmed.at](http://www.biotechmed.at)). Armin Lechleiter, University of Bremen, Center for Industrial Mathematics, Germany.

---

© 2019 Copyright held by the owner/author(s). Publication rights licensed to ACM.

This is the author's version of the work. It is posted here for your personal use. Not for redistribution. The definitive Version of Record was published in *ACM Transactions on Mathematical Software*, <https://doi.org/10.1145/3328525>.

As a special case of a nonlinear, ill-posed parameter identification problem it is notoriously difficult to solve. Furthermore, the discretization of the problem leads to a large system of equations, which makes the problem even more challenging to treat computationally.

Despite the various, aforementioned applications, there are—to the authors’ best knowledge—only two software packages dealing with the inverse medium problem: GLIDE, see [Strehlow 2014], and `sparseScatt` (a predecessor of `IPscatt`), see [Lechleiter et al. 2013]. The main reconstruction algorithm of GLIDE is based on a linearization of the underlying problem, which leads to suboptimal reconstructions, e.g. for relatively high wave numbers. The `sparseScatt` package on the other hand is based on a very time-consuming algorithm. Further, both packages have no implementation available to the general research community.

The main motivation behind `IPscatt` was to close this gap and to provide a free, open-source implementation of a reconstruction scheme for the nonlinear inverse medium problem in time-independent scattering in two and three dimensions.

The variational regularization scheme, on which the reconstruction part of `IPscatt` is based, was introduced in [Bürgel et al. 2017, Sec. 4] and relies on the so-called primal-dual algorithm due to Pock, Bischof, Cremers and Chambolle, see [Chambolle and Pock 2011; Pock et al. 2009]. In this *algorithm paper* we will show that the implementation of that scheme provided by `IPscatt` solves the underlying inverse medium problem efficiently and effectively.

To cope with the ill-posedness of the inverse problem we must add penalty terms, that are suited to a priori information about the contrast, see [Engl et al. 1996]. `IPscatt` achieves this by employing terms in the underlying regularization scheme that enforce sparsity in the pixel basis and are based on total variation as well as physical bounds. These terms were selected among other alternatives based on their combined effectiveness. However, if needed, all the necessary tools are provided within `IPscatt` to the user, who is interested in extending or altering the proposed reconstruction scheme. To the authors’ best knowledge, `IPscatt` is the first toolbox which provides such features and combines sparsity promoting and total variation-based regularization to jointly improve the reconstruction quality for the inverse medium problem.

This *algorithm paper* has three main aims: First, it gives an overview of the algorithms used in `IPscatt`. Second, it connects these algorithms with the implementation provided in the toolbox. Finally, by means of several, representative examples, it helps the interested reader to assess the efficiency and effectiveness of the software framework.

For further information on the details of `IPscatt` the reader may refer to the supplementary material<sup>1</sup>. It consists of the *source code*, the *source code documentation* for advanced usage and an *user guide* for `IPscatt`. The latter contains an installation guide, a technical description and a set of hands-on best practice recommendations and guides, e.g. how to simulate data avoiding the “inverse crime”.

The remainder of the paper is organized as follows: In Sec. 2 we give an overview of the software framework `IPscatt` and present its key features. In Sec. 3 we describe the direct scattering problem as well as the implemented variational reconstruction scheme and point out the main optimization features of `IPscatt`. Finally, in Sec. 4 we demonstrate the efficiency and effectiveness of `IPscatt` on several, representative examples. In particular, we compare `IPscatt` with other software packages.

Note as a preliminary remark that it does not matter, if simulated data, real-world data from Institute Fresnel or another real-world data set is used for the reconstruction of the contrast. Furthermore, `IPscatt` was not specifically designed to replace the used numerical solver from [Vainikko 2000] for the direct scattering problem. However, the modular and flexible design of `IPscatt` facilitates it. This requires two changes: the replacement of the forward operator and the forward

---

<sup>1</sup>Supplementary material is provided on <https://calgo.acm.org/> and on <http://www.fbuergel.de/ipscatt/> in the latest version.

operator's linearization (with the Fréchet derivative).<sup>2</sup> Indeed, a draft version of IPscatt was already modified by Lechleiter and Rennoch to tackle inverse scattering from so-called *anisotropic* penetrable media instead of *isotropic* penetrable media, see [Lechleiter and Rennoch 2017] or [Rennoch 2017, Ch. 3]. This opens up the opportunity to replace the used numerical solver by more sophisticated algorithms, see e.g. [Borges et al. 2017; Ying 2015]. In particular, this is interesting in the case of relatively high wave numbers. Note that IPscatt tackles the *single-frequency* inverse scattering problem in contrast to [Borges et al. 2017], that considers the *multi-frequency* case.

## 2 ARCHITECTURE AND KEY FEATURES OF IPSCATT

A typical MATLAB toolbox is a collection of functions/routines. If possible, object-oriented paradigms are not used or even avoided. In the design of IPscatt the authors have followed this common convention. Consequently, IPscatt is a collection of functions dealing with aspects of time-independent scattering.

*Groups of IPscatt.* Each of the functions provided by IPscatt can be put into one of the following five groups: *Initialization*, *Experimental Set-Up*, *Data Readers*, *Scattering Simulation* and *Contrast Reconstruction*. Each of these groups can be considered a module of the IPscatt toolbox. The connections between these groups can be found in Fig. 1. In the following paragraphs we discuss the tasks of each group.

The state of the algorithms employed in IPscatt is stored in a “master” data structure. The construction and initialization of that structure is carried out by the functions of the *Initialization* group. Several convenience functions, e.g. for loading of presets are included.

The *Experimental Set-Up* group is responsible for setting up the simulation grid and the positioning of the transmitters and receivers. Of course, many common transmitter-receiver geometries, like rectangle geometry, are provided by IPscatt, see Fig. 2(a). However, custom, user-defined geometries are supported too, see Fig. 2(b).

Further, the *Experimental Set-Up* group provides routines for the generation of predefined contrasts. In two dimensions these are e.g. a corner, a cross, a ball and a combination of two corners and one ball. IPscatt also provides routines for the generation of rotated variants of these contrasts. In three dimensions a tripod, a cross, a ball and the edges of a cube are available, see Fig. 2(c). Further, contrasts fitting to real-world data from Institute Fresnel, see [Belkebir and Saillard 2001], are contained: a contrast with one dielectric cylinder and another contrast with two dielectric cylinders.

The routines of the *Data Readers* read the real-world data from Institute Fresnel. Further, these routines are able to match the incident field for that data.

While the previous three groups are dealing with the preparation of the data structures necessary for the simulation and reconstruction, the fourth and fifth group, i.e. *Scattering Simulation* and *Contrast Reconstruction*, are the main power-horses of the toolbox.

*Scattering Simulation* provides the routines necessary for the simulation of the scattered fields at the receivers for a given contrast and a given transmitter-receiver geometry. This setting implicitly defines a nonlinear mapping of the contrast to the resulting fields. In what follows this mapping will also be called the *forward mapping* of the scattering. The details of this operator will be discussed in Sec. 3.

Further, the *Scattering Simulation* provides routines for the evaluation of the (Fréchet) derivative of that mapping as well as the derivative of the least-squares error of the forward mapping. The latter is provided since it is an important ingredient of many reconstruction and optimization schemes,

<sup>2</sup>The existing parameter set `i_model`, that is used to distinguish between the Helmholtz equation in two and three dimensions (via `helmholtz2D` and `helmholtz3D`), helps with this task.

e.g. it is used in the thresholded, nonlinear Landweber, that bases on the so-called soft-shrinkage operator, see e.g. [Chan and Shen 2005].

We think that one of the many applications of `IPscatt` is to be a building block for simulation and reconstruction schemes for time-independent scattering. However, we are aware of the fact that some users may prefer to have a pre-packaged reconstruction scheme available. Therefore *Contrast Reconstruction* routines implement a variational reconstruction scheme. In it physically sensible contrasts are reconstructed from measured fields at the receivers. The underlying reconstruction scheme is based on the assumption that such contrasts admit sparsity, total variation and physical bounds properties. It works in two- as well as three-dimensional setting, see Fig. 2(d). We have carried out extensive numerical experiments to tune the parameters of that scheme ensuring its effectiveness and efficiency.

*Supplementary Material.* The interested user will find a detailed description of the provided routines in the *source code documentation* of `IPscatt`. The main cornerstones of the discretization approach and the variational reconstruction provided by `IPscatt` are presented and discussed in a more condensed form in Sec. 3. Here, we would also like to mention the *user guide* of `IPscatt`, where many typical use cases, like the loading of and the working with real-world data from Institute Fresnel or the matching of the incident fields from receivers' measurements are described.

*Key Features.* Altogether, the *key features* of `IPscatt` can be summarized as follows:

- simulation of the time-independent scattering/the forward mapping of scattering,
- (Fréchet) derivative of the forward mapping,
- derivative of the least-squares error of the forward mapping,
- a reconstruction scheme of the contrast from measured fields,
- predefined and user-defined transmitter-receiver geometries,
- predefined and user-defined contrasts in 2D and 3D,
- detailed *user guide* and *source code documentation*.

### 3 SIMULATION AND RECONSTRUCTION

In this section we take a closer look at the already-mentioned main power-horses of `IPscatt`: the function groups *Scattering Simulation* and *Contrast Reconstruction*.

In the first and second part of this section we describe the mathematical model of time-independent scattering employed by `IPscatt`, i.e. the direct scattering problem. It consists of three steps: initially, a transmitter propagates a field into a region containing the obstacle. Then that obstacle, which is expressed by the contrast

$$q := n^2 - 1 \quad \text{with } n \text{ as refractive index,} \quad (1)$$

scatters that field in that region. Finally, the scattered field is propagated towards receivers, which measure it. In mono-static setting the related operator maps a contrast to the resulting near or far field operator. In the multi-static case the analogue is considered, i.e. the mapping of the contrast to the field operators for all transmitters, cf. Fig. 3(a). We denote in both cases the involved *forward operator* by  $\mathcal{F}$  and concentrate on the multi-static case in our formulations. We will also discuss the Fréchet derivative of the forward operator and its adjoint. We are relatively brief regarding theoretical properties of any introduced quantity and refer to [Bürgel et al. 2017, Secs. 2 and 3] as well as [Colton and Kress 2013] for details. However, we offer the essential formulas of the direct scattering problem in the continuous and discretized form to get an overview and get familiar with the used notation.

The first part of this section contains the continuous formulation of the direct scattering problem and the second part its discretization. A tabular of all involved formulas can also be found in the

*user guide*, where also a connection between mathematical formulas and their implementation is built. In the third part of this section we consider the variational reconstruction scheme used in IPscatt to solve the inverse problem. Finally, the last part discusses the complexity issues of IPscatt.

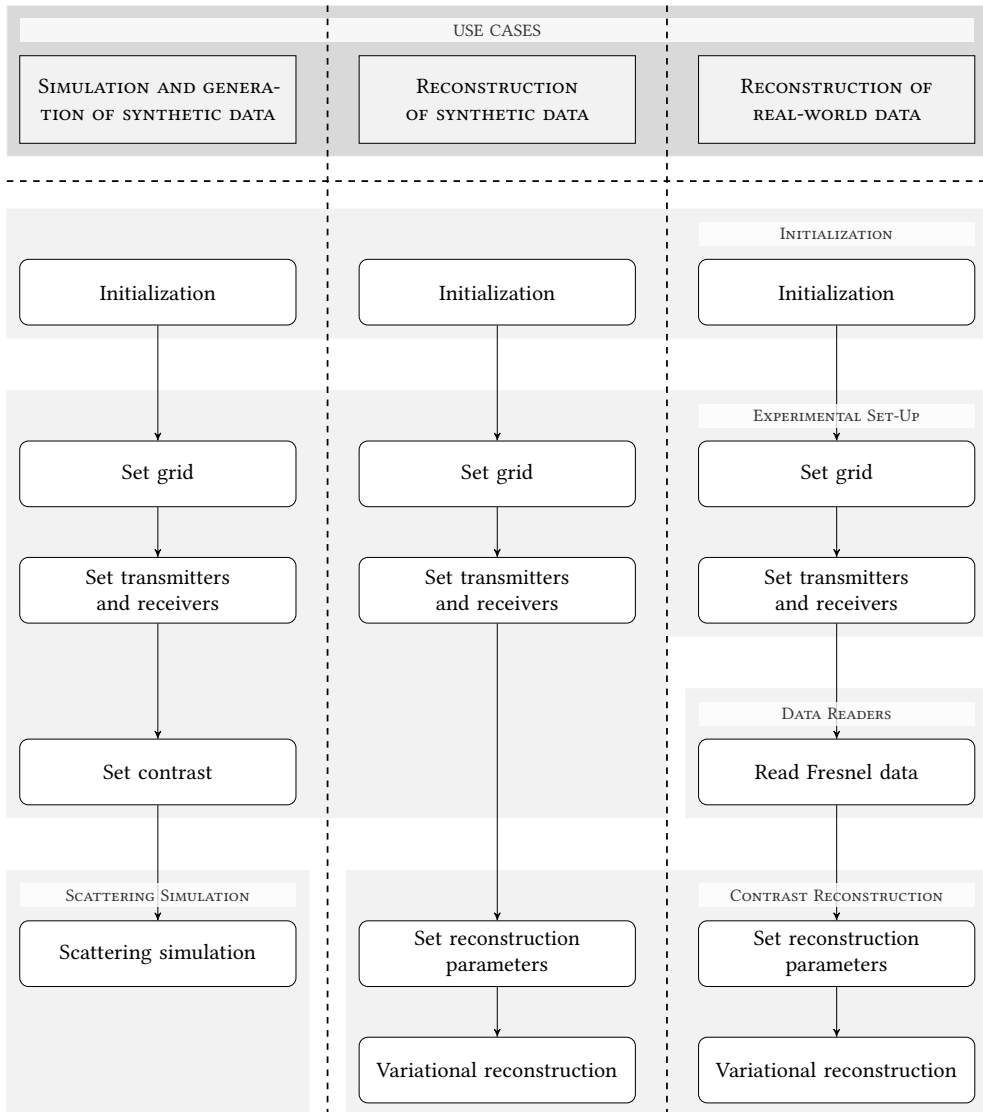


Fig. 1. Typical use cases of IPscatt and their connection to the modules/function groups *Initialization*, *Experimental Set-Up*, *Data Readers*, *Scattering Simulation* and *Contrast Reconstruction*. Arrows indicate a typical data flow.

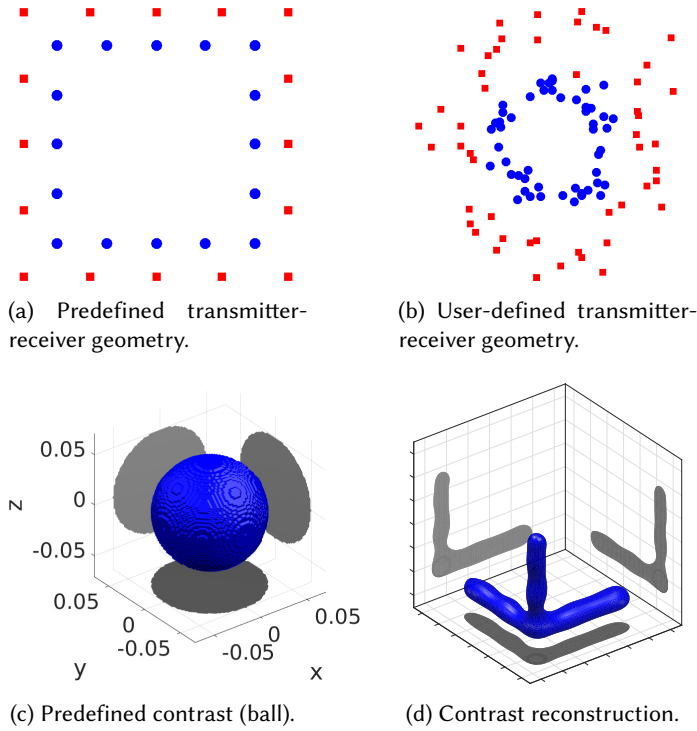


Fig. 2. Some key features of IPscatt. (a) Standard geometries for transmitters/receivers, available out of the box. (b) User-defined positions for transmitters/receivers. (c) Predefined contrasts in 2D and 3D. (Not shown are user-defined contrasts, which can also be used in IPscatt.) (d) Contrast reconstructions in 2D and 3D.

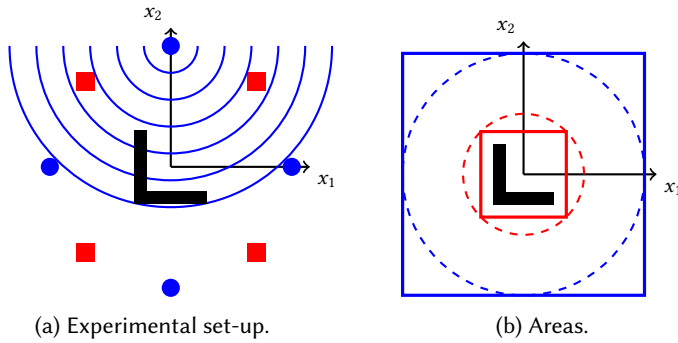


Fig. 3. (a) Experimental set-up for multi-static measurements: Transmitters (blue filled circles) propagate incident fields one after the other while the receivers (red filled squares) measure the generated fields scattered by an obstacle. (b) Areas: The square around the big circle with radius  $2R$  is the computational domain (CD),  $D_{2R} = [-2R, 2R]^2$ . The square inside the small circle with radius  $R$  is the region of interest (ROI),  $D = (-R/\sqrt{2}, R/\sqrt{2})^2$ . The corner inside the region of interest represents an obstacle  $G$ .

### 3.1 Direct Scattering Problem

In IPscatt we consider time-independent inverse scattering of incident waves  $u^i$  from an inhomogeneous medium in  $d = 2$  or  $d = 3$  dimensions. Omitting time-dependence  $\exp(-i\omega t)$ , where  $\omega$  is the angular frequency, the incident field  $u^i$  admits the Helmholtz equation  $\Delta u^i + k^2 u^i = 0$  for a wave number  $k > 0$ , which is the angular frequency divided by the speed of propagation. Typical choices of  $u^i$  include point sources and plane waves, defined after (4).

*Direct Scattering Problem.* If we denote by  $q: \mathbb{R}^d \rightarrow \mathbb{C}$  the compactly supported contrast and by  $\text{supp}(q) = \overline{G}$  its support, then the total field  $u^t$  solves

$$\Delta u^t + k^2(1 + q)u^t = 0 \quad \text{in } \mathbb{R}^d. \quad (2)$$

Further, the scattered wave  $u^s = u^t - u^i$  radiates away from the inhomogeneous medium, i.e.  $u^s$  satisfies Sommerfeld's radiation condition

$$\lim_{|x| \rightarrow \infty} |x|^{(d-1)/2} \left( \frac{\partial}{\partial |x|} - ik \right) u^s(x) = 0, \quad \text{uniformly in all directions } \hat{x} = x/|x|. \quad (3)$$

The direct scattering problem is to find a  $u^s$  solving (2) and (3), or, equivalently, to find a radiating solution to the equation  $\Delta u^s + k^2(1 + q)u^s = -k^2 q u^i$ . Note that the support of the right-hand side equals  $\overline{G}$  (unless the incident field vanishes). Unique solvability of the scattering problem holds whenever the contrast  $q$  is smooth enough such that a unique continuation principle holds, and in particular if  $q$  is bounded, see [Colton and Kress 2013].

The direct scattering problem describes waves with fixed frequency that are interacting with a penetrable inhomogeneous medium, both in two and three dimensions. It models two physical settings: first, the scattering of acoustic waves and second, the scattering of electromagnetic waves in transverse magnetic (TM) polarization from some non-magnetic material, see e.g. [Colton and Kress 2013].

*Reformulation of the Direct Scattering Problem.* We denote by  $\Phi$  the radiating fundamental solution of the Helmholtz equation,

$$\Phi(x) = \frac{i}{4} H_0^{(1)}(k|x|) \quad \text{if } x \in \mathbb{R}^2 \setminus \{0\}, \quad \Phi(x) = \frac{1}{4\pi} \frac{e^{ik|x|}}{|x|} \quad \text{if } x \in \mathbb{R}^3 \setminus \{0\}, \quad (4)$$

where  $H_0^{(1)}$  is the Hankel function of the first kind and order zero, see [Abramowitz and Stegun 1965, Ch. 9]. Typical models of the incident waves  $u^i$  are the real part of a point source, i.e.  $u^i(x) = \Phi(x-p)$  with origin in  $p \in \mathbb{R}^d$ , and the real part of a plane wave, i.e.  $u^i(x) = e^{ikx \cdot \theta}$  with  $\theta$  as the direction of propagation.

Further, we define for the domain  $D \supset \overline{G}$  the radiating volume potential

$$v(x) := (Vf)(x) := k^2 \int_D \Phi(x-y)f(y) \, dy, \quad x \in \mathbb{R}^d. \quad (5)$$

The volume potential operator  $V$  defines the radiating solution  $v = Vf$  of the Helmholtz equation  $\Delta v + k^2 v = -k^2 f$  in  $\mathbb{R}^d$ , such that the direct scattering problem can be equivalently reformulated as follows: Find a scattered field  $u^s$  solving the so-called Lippmann-Schwinger integral equation

$$u^s - V(q \cdot u^s) = V(q \cdot u^i) \quad \text{for } x \in D. \quad (6)$$

Note that we use the notation  $f \cdot g$  if we want to stress the pointwise multiplication. In general the set  $D$  is assumed to be only slightly larger than the support of the contrast,  $\overline{G}$ , and is called the *region of interest* because we know that the scattering takes place inside.

Further, the Lippmann-Schwinger equation implicitly defines the Lippmann-Schwinger solution operator  $T_q$  mapping  $u^i$  to  $u^t$  on  $D$  via

$$T_q: L^2(D) \rightarrow L^2(D), \quad T_q := (I - V(q \cdot))^{-1}, \quad (7)$$

where the notation  $(q \cdot)$  is used to denote the operator of pointwise multiplication (with a function  $q$ ).

*Incident Field and Scattered Field.* Next, we need to clarify the model for the generation of the incident field and the measurement of the scattered field. For the first part, we will present only the case of point sources. However, we remark that `IPscatt` can also handle the case of sources being plane waves. For point sources one assumes that the transmitters generating the field are located on some surface  $\Gamma_i$  in  $\mathbb{R}^d \setminus \bar{G}$ . Then, the so-called single-layer potential, see [Colton and Kress 2013, Sec. 3.1],

$$\text{SL}_{\Gamma_i \rightarrow D}: L^2(\Gamma_i) \rightarrow L^2(D), \quad (\text{SL}_{\Gamma_i \rightarrow D} g)(x) := \int_{\Gamma_i} \Phi(x - y)g(y) ds(y), \quad x \in D \setminus \Gamma_i \quad (8)$$

models the incident field via  $u^i = \text{SL}_{\Gamma_i \rightarrow D} g$  with density  $g$ .

*Scattering Process.* As mentioned above, this field generated on  $\Gamma_i$  propagates into the region of interest  $D$  and interacts there with the contrast  $q$  via the Lippmann-Schwinger solution operator  $T_q$ . Next, the resulting fields  $u^t$  respectively  $u^s$  propagate out of  $D$  and can be measured. It is known that the scattered field  $u^s$  has the asymptotic behavior

$$u^s(x) = \frac{\exp(ik|x|)}{|x|^{(d-1)/2}} \left( u^\infty(\hat{x}) + \mathcal{O}\left(\frac{1}{|x|}\right) \right) \quad \text{as } |x| \rightarrow \infty, \text{ uniformly in all directions } \hat{x} = x/|x| \in \mathbb{S}^{d-1}.$$

Therefore only the so-called far field  $u^\infty: \mathbb{S}^{d-1} \rightarrow \mathbb{C}$  is measured in direction  $\hat{x}$  if the receivers are located far away from  $G$ . In contrast, if the receivers are near  $G$ , it is advantageous to model the receivers as measuring the near field  $u^s(x)$ . We remark that `IPscatt` can handle both cases, however, in what follows we only discuss the near field case for the sake of brevity. Let  $\Gamma_s$  in  $\mathbb{R}^d \setminus \bar{G}$  be a surface on which the receivers are located. Then a field  $f$  given on  $D$  can be propagated onto  $\Gamma_s$  via the solution-to-data operator

$$V_{D \rightarrow \Gamma_s}: L^2(D) \rightarrow L^2(\Gamma_s), \quad (V_{D \rightarrow \Gamma_s} f)(x) := k^2 \int_D \Phi(x - y)f(y) dy, \quad x \in \Gamma_s. \quad (9)$$

The data at a particular receiver on  $\Gamma_s$  of the resulting field is modeled as pointwise evaluation at the related position  $x$ . Altogether, the introduced operators can be used to model the whole scattering process via the forward operator

$$\mathcal{F}(q) := V_{D \rightarrow \Gamma_s}(q \cdot) T_q \text{SL}_{\Gamma_i \rightarrow D}. \quad (10)$$

A sensible domain and range of the operator are given via  $\mathcal{F}: L^p_{\text{Im} \geq 0}(D) \rightarrow \text{HS}$ , where HS is the space of all Hilbert-Schmidt operators  $\text{HS}(L^2(\Gamma_i), L^2(\Gamma_s))$ . This operator is nonlinear in  $q$  since the Lippmann-Schwinger solution operator  $T_q$  is so. However, the evaluation of  $\mathcal{F}$  at  $q$  is a linear operator mapping a transmitter density  $g$  on  $\Gamma_i$  to the resulting field on  $\Gamma_s$ . Further, it is clear from the above considerations that the forward operator depends on the incident field type, the positions of the transmitters respectively the outgoing directions, the measurement model (near field or far field data) and the positions respectively directions of the receivers.

For the sake of completeness, we give the Fréchet derivative of the forward operator  $\mathcal{F}$  because it is an important ingredient of many reconstruction and optimization schemes (if it is applied to the defect),

$$\mathcal{F}'(q): L^2(D) \rightarrow \text{HS}, \quad \mathcal{F}'(q)[h]g = V_{D \rightarrow \Gamma_s}(I + (q \cdot)T_q V)(h \cdot)T_q \text{SL}_{\Gamma_i \rightarrow D} g, \quad g \in L^2(\Gamma_i). \quad (11)$$



*Numerical Solution.* For a numerical solution of the forward operator we essentially follow [Vainikko 2000]. The basic idea is to exploit the convolution structure of the volume potential operator  $V$ , see (5), consisting of the radiating fundamental solution  $\Phi$ , see (4), and a function  $f$ , say, on  $B_R$  (ball with radius  $R$ ) for some fixed radius  $R > 0$ . Therefore this operator can in Fourier space be represented as the element-wise product of the Fourier coefficients of both functions. This is the key for an efficient solution of the Lippmann-Schwinger equation (6) on an equidistant grid via the fast Fourier transform (FFT). This equidistant grid of the computational domain  $D_{2R}$ , defined in (12), is denoted by  $\text{CD} = \mathbb{C}_N^d$ . More precisely, the periodized volume potential operator  $V_{2R}$ , defined in (13), allows to consider in the computational domain  $D_{2R}$  the periodized Lippmann-Schwinger equation corresponding to (6),

$$v - V_{2R}(q \cdot v) = V_{2R}(q \cdot u^i) \quad \text{in } L^2(D_{2R}).$$

Fourier coefficients of the convolution kernel can be explicitly computed, see [Vainikko 2000]. Finally, we use GMRES algorithm to solve the arising discrete linear system efficiently.

Starting from radius  $R$  the computational domain (CD) is the smallest square/cube around the circle/ball with radius  $2R$ , i.e.

$$D_{2R} = [-2R, 2R)^d \subset \mathbb{R}^d, \quad (12)$$

see Fig. 3(b). The corresponding equidistant grid of  $D_{2R}$  is  $\text{CD} = \mathbb{C}_N^d$  with mesh size  $h_N = 4R/N$ . Following [Vainikko 2000] it is sufficient to evaluate the volume potential (5) on this computational domain  $D_{2R}$  instead of  $\mathbb{R}^d$ . Therefore in the following we consider the periodized volume potential operator

$$V_{2R}: L^2(D_{2R}) \rightarrow L^2(D_{2R}), \quad (V_{2R}f)(x) := \int_{D_{2R}} \Phi_{2R}(x-y)f(y) dy, \quad x \in D_{2R}, \quad (13)$$

where the modified kernel  $\Phi_{2R}(x)$  in the computational domain is  $k^2\Phi(x)$  if  $x \in \overline{B_{2R}}$  and 0 if  $x \in \overline{D_{2R}} \setminus \overline{B_{2R}}$ . IPscatt uses further improvements to evaluate the Lippmann-Schwinger equation (6) efficiently. One of these is the restriction of all unknowns and all data to the already-mentioned region of interest (ROI), that is the biggest square/cube inside the circle/ball with radius  $R$ , i.e.  $D = (-R/\sqrt{2}, R/\sqrt{2})^d$  (the definition in [Bürigel et al. 2017] was corrected), see Fig. 3(b); the corresponding equidistant grid of  $D$  is  $\text{ROI} = \mathbb{C}_{N_D}^{N_D}$  with  $N_D := \lfloor N/(2\sqrt{2}) \rfloor^d$ ; again, see [Bürigel et al. 2017] for details.

Actually, the region of interest should be the mathematical sensible region, i.e.  $B_R$ , however, the chosen square/cube  $D \subset B_R$  as region of interest is easier to implement than a circle/ball and can be used as long as it is ensured that  $\overline{D}$ , i.e. the support of the contrast  $q$ , is inside  $D$ .

### 3.2 Discretization

Next, we discuss the discretization of the scattering problem. That concerns the discretization of the single-layer potential  $\text{SL}_{\Gamma_i \rightarrow D}$ , the volume potential operator  $V$ , the solution-to-data operator  $V_{D \rightarrow \Gamma_s}$ , the Lippmann-Schwinger solution operator  $T_q$  and finally the forward operator  $\mathcal{F}$ . In addition, for practical usage we give the Fréchet derivative of the forward operator and its adjoint.

As we have used the notation  $f \cdot g$  to stress the pointwise multiplication in the continuous case we use  $f \odot g$  in the discretized one. Where sensible we use underline to denote a discretized version of a continuous quantity.

*Single-Layer Potential.* The single-layer potential (8) for  $N_i$  source points at  $p_j$  is discretized via

$$\text{SL}_{N_i, N_D} : \mathbb{C}^{N_i} \rightarrow \mathbb{C}^{N_D}, \quad \text{SL}_{N_i, N_D} := \Phi_{\text{SL}}(\omega^i \odot),$$

where  $(\Phi_{\text{SL}})_{\ell,j} := \Phi(x_\ell - p_j)$  with  $\ell = 1, \dots, N_D$  and  $j = 1, \dots, N_i$  is the collocation of the transmitted field and  $\omega_j^i \approx \text{ds}(p_j)$  are the approximations of the infinitesimal element on  $\Gamma_i$ .

One notices in the continuous formulation of the single-layer potential (8) the required absence of point sources inside the region of interest  $D$  because the singularity of the radiating fundamental solution (4) at the origin. This restriction is irrelevant in the discretized version as long as the transmitter is not near a grid point.

*Volume Potential Operator.* The periodized volume potential operator  $V_{2R}$ , see (13), is discretized via

$$V_{N_D} : \mathbb{C}^{N_D} \rightarrow \mathbb{C}^{N_D}, \quad V_{N_D} := \mathcal{R}_N \text{FFT}_N^{-1} (\widehat{\Phi}_N \odot) \text{FFT}_N \mathcal{E}_N,$$

where  $\mathcal{E}_N : \mathbb{C}^{N_D} \rightarrow \mathbb{C}_N^d$  and  $\mathcal{R}_N : \mathbb{C}_N^d \rightarrow \mathbb{C}^{N_D}$  are the discretizations of the extension and restriction operators from the region of interest to the computational domain. Further,  $\text{FFT}_N = \text{fft2}$  and  $\text{FFT}_N^{-1} = \text{ifft2}$  are the forward and inverse fast Fourier transforms with the common normalization constants as used in MATLAB. Finally,  $\widehat{\Phi}_N$  denotes the Fourier coefficients of the fundamental solution stored in FFT convention, i.e. the constant term being at matrix position  $(1, 1)$ .

*Solution-to-Data Operator.* The solution-to-data operator (9) is discretized via

$$V_{N_D, N_s} : \mathbb{C}^{N_D} \rightarrow \mathbb{C}^{N_s}, \quad V_{N_D, N_s} := h_N^d k^2 \Phi_V,$$

where the exact form of the kernel  $\Phi_V$  depends on whether near or far field data is being measured and on the positions of the receivers  $x_\ell$  with  $\ell = 1, \dots, N_s$  respectively their directions. Further,  $h_N^d$  is the approximation of the ROI's infinitesimal element. One notices that there is no restriction for receivers' positions as long as they are not in  $\overline{G}$ .

*Forward Operator.* Finally, the Lippmann-Schwinger solution operator (7) is discretized via

$$T_{\underline{q}} : \mathbb{C}^{N_D} \rightarrow \mathbb{C}^{N_D}, \quad T_{\underline{q}} := (I - V_{N_D}(\underline{q} \odot))^{-1} \quad (14)$$

with  $\underline{q} \in \mathbb{C}^{N_D}$ . Altogether, the discretized forward operator (10) is given via

$$\underline{\mathcal{F}} : \mathbb{C}^{N_D} \rightarrow \mathbb{C}^{N_s \times N_i}, \quad \underline{\mathcal{F}}(\underline{q}) := V_{N_D, N_s}(\underline{q} \odot) T_{\underline{q}} \text{SL}_{N_i, N_D}. \quad (15)$$

The resulting Fréchet derivative of the forward operator, (11), is given via, see [Bürgel et al. 2017, Sec. 3.6],

$$\underline{\mathcal{F}}'(\underline{q}) : \mathbb{C}^{N_D} \rightarrow \mathbb{C}^{N_s \times N_i}, \quad \underline{\mathcal{F}}'(\underline{q})[\underline{h}] = A_{N_D, N_s}(\underline{h} \odot) B_{N_D, N_i}, \quad \underline{h} \in \mathbb{C}^{N_D} \quad (16)$$

with auxiliary matrices

$$\begin{aligned} A_{N_D, N_s} &= V_{N_D, N_s} (I + (\underline{q} \odot) T_{\underline{q}} V_{N_D}) \in \mathbb{C}^{N_s \times N_D}, \\ B_{N_D, N_i} &= T_{\underline{q}} \text{SL}_{N_i, N_D} \in \mathbb{C}^{N_D \times N_i}. \end{aligned}$$

Its adjoint is then given via

$$[\underline{\mathcal{F}}'(\underline{q})]^* : \mathbb{C}^{N_s \times N_i} \rightarrow \mathbb{C}^{N_D}, \quad [\underline{\mathcal{F}}'(\underline{q})]^* \underline{H} = \sum_{j=1}^{N_s} \sum_{\ell=1}^{N_i} \underline{H}_{j,\ell} \overline{A_{N_D, N_s}(j, \cdot) B_{N_D, N_i}(\cdot, \ell)}, \quad \underline{H} \in \mathbb{C}^{N_s \times N_i}.$$

The adjoint applied to the defect  $\mathcal{F}(q) - F_{\text{meas}}^\delta$  is the derivative of the least-squares error of the forward operator and as already mentioned is an important ingredient of many reconstruction and optimization schemes. Note that all spaces for the discretized operators are equipped with the usual non-weighted  $\ell^2$  norms.

### 3.3 Variational Reconstruction

As mentioned previously *Contrast Reconstruction* is one of the main five components of IPscatt. In this section we present a brief introduction to the mathematical formulation of the inverse scattering problem and the implemented variational reconstruction scheme, cf. [Bürigel et al. 2017, Sec. 4] for more details. We would like to remind that the variational approach uses sparsity, total variation and physical bounds as penalty terms. We start by introducing the typical terminology used in the context of parameter identification respectively inverse scattering problems.

*Data.* To that end, the scattered field at the receivers' positions is called *data*. Further, simulated data with noise (or real-world data) is denoted by  $F_{\text{meas}}^\delta$ , where  $\delta$  is the relative noise level. Consequently, simulated data without noise is denoted by  $F_{\text{meas}}$ . For the sake of completeness, we mention that the synonym *exact data* for  $F_{\text{meas}}$  is used in the *user guide* and in the *source code*.

*The Inverse Scattering Problem.* For a description of the inverse scattering problem we recall the nonlinear forward operator  $\mathcal{F}$ , see (10) respectively (15), and consider the discretized version: The operator  $\mathcal{F}$  maps the contrast  $q \in \mathbb{C}^{N_b}$  onto perturbed near or far field data  $F_{\text{meas}}^\delta \in \mathbb{C}^{N_s \times N_t}$ , where  $N_s$  is the number of receivers and  $N_t$  the number of transmitters. In the context of contrast reconstruction the task is to find a contrast  $q$  such that  $\mathcal{F}(q)$  matches the data  $F_{\text{meas}}^\delta$  as good as possible. Since the underlying problem is ill-posed, a sensible reconstruction can be computed by minimizing the following Tikhonov functional with a Frobenius norm  $\|\cdot\|_F$  and penalty terms in the convex functional  $\mathcal{P}$ ,

$$q \mapsto \frac{1}{2} \|\mathcal{F}(q) - F_{\text{meas}}^\delta\|_F^2 + \mathcal{P}(q). \quad (17)$$

*Penalty Terms.* To take into account three kinds of a priori information about the contrast, the ansatz for  $\mathcal{P}(q)$  is the sum of the following three penalty terms: First, the contrast is assumed to be sparse, i.e. described by few non-zero coefficients, in the pixel basis. This is taken into account by a penalty term weighted by a regularization parameter  $\alpha > 0$ ,  $\alpha \|q\|_1$ . Second, the scattering object is supposed to have sharp edges. Thus, the total variation semi-norm is added as a penalty term using the notation  $\beta \|\nabla q\|_1$ , where  $\beta > 0$  is an additional regularization parameter. Third, an indicator function  $\delta_{[a,b]}(q)$  is introduced, that equals infinity if one or more entries of  $q$  are outside a reasonable interval  $[a, b]$  and equals zero otherwise, to respect physical bounds of the real and imaginary part of the contrast by adding

$$\delta(q) = \delta_{[a,b]}(\text{Re}(q)) + \delta_{[c,d]}(\text{Im}(q)).$$

Altogether, the resulting penalty functional has the form

$$\mathcal{P}(q) = \alpha \|q\|_1 + \beta \|\nabla q\|_1 + \delta(q).$$

*Numerical Minimization Techniques.* The minimization of the Tikhonov functional (17) with the penalty functional discussed above is challenging because the forward operator  $\mathcal{F}$  is nonlinear. Therefore we use the typical approach for ill-posed problems: linearization and iteration. So, the linearization of  $\mathcal{F}$  leads us to consider  $d_q(h) := \|\mathcal{F}'(q)[h] + \mathcal{F}(q) - F_{\text{meas}}^\delta\|_F$  instead of the discrepancy  $d(q) := \|\mathcal{F}(q) - F_{\text{meas}}^\delta\|_F$ . This results in an extension of the Tikhonov functional (17) to  $f_q(h) := \frac{1}{2} [d_q(h)]^2 + \mathcal{P}(q+h)$ . Finally, the minimization functional is given by

$$\min_{h \in \mathbb{C}^{N_b}} \underbrace{\frac{1}{2} \|\mathcal{F}'(q)[h] + \mathcal{F}(q) - F_{\text{meas}}^\delta\|_F^2}_{=: f_{\text{dis}}(h)} + \underbrace{\alpha \|q+h\|_1}_{=: f_{\text{sps}}(h)} + \underbrace{\beta \|\nabla(q+h)\|_1}_{=: f_{\text{tv}}(h)} + \underbrace{\delta(q+h)}_{=: f_{\text{phy}}(h)}. \quad (18)$$

The minimization of that functional is tackled by the primal-dual algorithm, see [Chambolle and Pock 2011], which consists of two fixed-point iterations and an over-relaxation step. The summands

are the discrepancy of the linearized problem  $f_{\text{dis}}(h)$ , the sparsity penalty  $f_{\text{spa}}(h)$ , the total variation penalty  $f_{\text{tv}}(h)$  and the physical bounds  $f_{\text{phy}}(h)$ . We take up these terms and symbols in the *user guide* as well as the *source code* and they already occurred in [Bürgel et al. 2017].

Then an iterative update for  $h$  is used as the second ingredient of the variational scheme.

Note that (18) is a simplified formulation of the actual minimization functional: actually, first, the norms are weighted to model precisely the experimental set-up and second, to deal with complex-valued contrasts a transformation into real-valued ones is inserted, such that all requirements of the underlying primal-dual algorithm are satisfied; more information is given in the *source code documentation* of the routine `setFuncsPda`.

It is well-known that the primal-dual algorithm requires the splitting of the minimization functional (18) into two parts  $F$  and  $G$  with  $\min_{h \in \mathbb{C}^{\mathcal{N}_D}} F(Kh) + G(h)$ , where  $K$  is a continuous linear operator, see [Chambolle and Pock 2011]. Different choices for  $F$  and  $G$  are possible in the case of (18). However, as elaborated in [Bürgel et al. 2017] the following approach was employed

$$F(Kh) = f_{\text{dis}}(h) + f_{\text{tv}}(h) \quad \text{and} \quad G(h) = f_{\text{spa}}(h) + f_{\text{phy}}(h). \quad (19)$$

*Variational Reconstruction Scheme.* Finally, we give an overview of the steps that the component *Contrast Reconstruction* processes. Afterwards we present stopping criteria for the two iterative parts of the reconstruction algorithm. For a full pseudo code of the variational reconstruction scheme with all technical details like the corresponding proximal mappings we refer to [Bürgel et al. 2017, Sec. 4]. The scheme can be summarized as follows:

- (1) Initialization: Set the contrast  $q = 0$ .
- (2) Minimize  $f_q(h)$  with respect to  $h$ , i.e. (18), with the primal-dual algorithm given in [Chambolle and Pock 2011]. We call this iteration an *inner iteration*. If a stopping criterion is fulfilled, then go to step 3.
- (3) Update  $q := q + h$ . We call this linearization step an *outer iteration*. If a stopping criterion is fulfilled, then the variational reconstruction scheme ends.

*Stopping Criteria.* Both the inner and the outer iteration can be stopped after a fixed number of iterations. Following the best practice for inverse problems we recommend to stop the outer iteration by Morozov's discrepancy principle, i.e.

$$\text{if } d(q) / \|F_{\text{meas}}^\delta\|_{\text{F}} \leq \tau \delta \quad \text{with tolerance parameter } \tau > 1. \quad (20)$$

Further, we used extensive numerical experiments, see [Bürgel et al. 2017], to establish two heuristic strategies to stop the inner iteration and therefore provide them in `IPscat.t`. Both ensure that only a few inner iterations are executed inside the first outer iterations and allow a high number in later iterations. As will be demonstrated in Sec. 4 in ideal case a huge number of inner iterations is granted inside the last outer iteration to improve the reconstruction quality. The two strategies are as follows:

- (S1) Each time the inner iteration terminates the quantities  $d_q(h)$  and  $d(q + h)$  are compared. If they are similar, the number of inner iterations is increased, otherwise it is decreased.
- (S2) Inside the inner iteration the quantities  $d_q(h)$  and  $d(q)$  are compared. If they are similar, the inner iteration is terminated. (This strategy follows an inexact stopping rule for a Newton-like method, see [Rieder 2001].) We realize that it would be interesting to compare  $d_q(h)$  and  $d(q + h)$  directly, however, this involves an additional evaluation of the forward operator  $\mathcal{F}$ , which was deemed too expensive for the purpose of a stopping criterion.

### 3.4 Complexity

In this section we discuss the computational cost and main optimizations of the function groups *Scattering Simulation* and *Contrast Reconstruction*.

*Scattering Simulation.* As can be seen in (10) and (15) the evaluation of the forward operator consists of the single-layer potential, the data-to-solution operator and the evaluation of the Lippmann-Schwinger solution operator  $T_q$ , see (7) respectively (14). The latter is equivalent to the solution of the Lippmann-Schwinger equation (6).

The discretization of the first two operators (single-layer potential and data-to-solution operator) consists of a matrix multiplication and therefore their computational cost is negligible. However, the efficient solution of the Lippmann-Schwinger equation is more challenging.

Following [Vainikko 2000] the domain of the operator is periodized and the collocation method is applied. Therefore the convolution structure of the periodized volume potential operator  $V_{2R}$ , see (13), is exploited and Fourier coefficients are used. Further, using FFT lowers the number of floating-point operations from  $N^{2d}$  to  $O(N^d \log N)$ , where  $N$  is the number of discretization points in each dimension  $d$ . In contrast to [Vainikko 2000] IPscatt stores the necessary Fourier coefficients such that unnecessary shift operations (and therefore memory operations) are avoided. As already mentioned appropriate restriction and extension operators are used to lower the memory footprint. In particular, all quantities outside of the periodized volume potential operator  $V_{2R}$  are only stored within the region of interest  $D$  instead of the whole computational domain  $D_{2R}$ . Finally, IPscatt solves the underlying system of linear equations with the GMRES from Kelley, see [Kelley 1995, Sec. 3.4] and [Kelley 2002] for the source code. In our numerical experiments this solver turned out to be superior to standard GMRES.

*Contrast Reconstruction.* In the case of the *Contrast Reconstruction* the forward operator must be evaluated and auxiliary matrices for the Jacobian matrix (Fréchet derivative) of the forward operator are required, see (16). These two preparations (forward operator and auxiliary matrices) for the inner iterations are time consuming. We remark that each of the steps of the inner iteration, i.e. each of the steps in the primal-dual algorithm, see [Chambolle and Pock 2011], has a small computational effort. However, for a sufficiently good reconstruction a large number of these steps is necessary. Therefore the overall cost of these iterations is considerable.

As already mentioned, IPscatt provides the derivative of the least-squares error of the forward operator although it is not part of our reconstruction scheme. Its computational cost is reasonable because it can be computed without evaluating the full derivative first. Further, IPscatt reduces the overall computational effort of reconstruction schemes using the forward operator as well as the derivative of the least-squares error by evaluating both in one routine.

## 4 EXAMPLES

In this section we demonstrate the main applications of IPscatt using representative examples. Further, we compare IPscatt with two other software packages (sparseScatt and GLIDE) performing the same task, i.e. solving the inverse medium problem in scattering, and we discuss the advantages of IPscatt over these packages.

In this regard, we put the *Contrast Reconstruction* in the foreground because the essential differences among the three packages are in this group. As mentioned before, *Contrast Reconstruction* is only one of the five function groups of IPscatt apart from *Initialization*, *Experimental Set-Up*, *Data Readers* and *Scattering Simulation*. However, we will choose the test cases such that all other function groups are implicitly included in at least one of the discussed examples.

#### 4.1 Comparing Software Packages

We begin our discussion with a survey of the reconstruction methods implemented by the software packages `sparseScatt` and `GLIDE` and refer to [Lechleiter et al. 2013] respectively [Strehlow 2014, Ch. 5] for details.

*Package sparseScatt.* The package `sparseScatt` solves the nonlinear inverse medium problem in scattering using a thresholded, nonlinear Landweber method, which employs the so-called soft-shrinkage operator, see e.g. [Chan and Shen 2005]. In `sparseScatt` the contrast is assumed to be sparse with respect to the pixel basis. Therefore the underlying Tikhonov functional is given by

$$\min_{q \in \mathbb{C}^{N_D}} \frac{1}{2} \|\mathcal{F}(q) - F_{\text{meas}}^\delta\|_F^2 + \alpha \|q\|_1. \quad (21)$$

*Package GLIDE.* The package `GLIDE` relies on the Born approximation on the physical model of scattering. The Born approximation can be considered as the linearization of the forward operator (10) in the origin, cf. [Born 1926]. Further, for the reconstruction the contrast is assumed to be sparse. However, in contrast to `IPscatt` and `sparseScatt` the sparsity is assumed to be with respect to a wavelet basis, e.g. the Cohen-Daubechies-Feauveau-9/7 (CDF) wavelets. Finally, the related variational problem is solved via the *fast iterative shrinkage-thresholding algorithm for linear inverse problems* (FISTA), see [Beck and Teboulle 2009].

*Package IPscatt.* To the best of our knowledge, `IPscatt` is the first freely available software package providing an advanced contrast reconstruction scheme in two and three dimensions, providing data handling routines for real-world data from Institute Fresnel and finally, providing several transmitter-receiver geometries.

#### 4.2 Experimental Set-Ups

For our experiments we will consider the three transmitter-receiver geometries shown in Fig. 4, that we call *Fresnel case*, *borehole case* and *sphere case*.

*Fresnel Case.* In the *Fresnel case*, we use the same experimental set-up as in [Strehlow 2014, Sec. 5.5, Fig. 5.6], i.e. we consider scattering in two dimensions with a contrast consisting of a plane of two homogeneous, long cylindrical dielectrics, see Fig. 5(a)/(e). This is the same set-up as used in the real-world data set `twodie1TM_8f.exp` from Institute Fresnel, see [Belkebir and Saillard 2001]. There are 36 transmitters arranged on a circle with radius  $720 \pm 3$  mm. Each of these point sources emits an electromagnetic wave in TM polarization with a frequency of 6 GHz, i.e. wave number  $k \approx 126 \text{ m}^{-1}$ . The 72 receivers are arranged on a circle with radius  $760 \pm 3$  mm. The experimental set-up is depicted in Fig. 4(a). We would like to point out that for metrological reasons some transmitter-receiver links are missing, i.e. the discretized forward operator  $\mathcal{F}$ , see (15), maps from  $\mathbb{C}^{N_D}$  to an appropriate subspace of  $\mathbb{C}^{N_s \times N_r}$ . Therefore the minimization functional (18) was adapted accordingly.

*Borehole Case.* In the *borehole case*, we consider a synthetic contrast in two dimensions consisting of a real and an imaginary part as depicted in Fig. 6(a)/(e). The contrast was constructed to be challenging as it consists of a gradual contrast ramp (the thick horizontal rectangle at the bottom of the real and imaginary part of the contrast) as well as fine features (a filled circle, small squares with different contrasts in real as well as imaginary part and a rotated thin line in the real part). The transmitter-receiver geometry consists of two boreholes 10 m apart and 20 m deep. Each borehole is assumed to be equipped with 18 transmitters and receivers, that are arranged in the configuration presented in Fig. 4(b). The transmitters are assumed to be point sources emitting with a wave

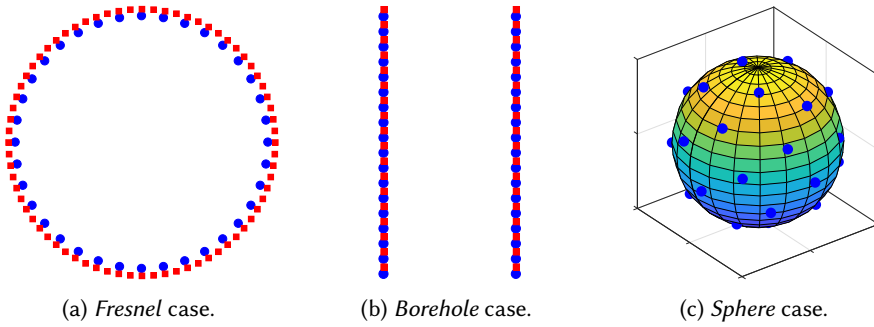


Fig. 4. Experimental set-ups for comparisons. Transmitters are blue filled circles and receivers red filled squares. (a) *Fresnel case*: Transmitters and receivers are arranged on circles as in the experimental set-up of Institute Fresnel, see [Belkebir and Saillard 2001]. (b) *Borehole case*: Transmitters and receivers are arranged on two boreholes. (c) *Sphere case*: Transmitters (and receivers) are roughly equidistantly arranged on a sphere.

number  $k = 250 \text{ m}^{-1}$ , i.e. a frequency of 11.9 GHz. Gaussian noise with noise level of 1% in real and imaginary part was employed to simulate data in this case.

*Sphere Case.* In the *sphere* case, three-dimensional scattering is considered. The synthetic contrast is depicted in Fig. 7(a)/(e). The transmitter-receiver geometry consists of 31 transmitters as well as receivers that are distributed almost equidistantly on the surface of a sphere with a radius of 5 m, see Fig. 4(c). To approximate an equidistant distribution the so-called Fibonacci lattice, see [González 2010, Sec. 3.1], was employed. The transmitters are point sources emitting with a wave number  $k = 10 \text{ m}^{-1}$ , i.e. a frequency of 0.5 GHz. Again 1% Gaussian noise was used in the data simulation.

### 4.3 Results and Discussion

*Results.* The results of the reconstructions in 2D are depicted in Figs. 5 and 6. The results in 3D are given in Fig. 7. We always show the contrast in the region of interest (ROI), i.e. it is a square approximately from  $-0.07 \text{ m}$  to  $0.07 \text{ m}$  in case of two dimensions and a cube from  $-0.70 \text{ m}$  to  $0.70 \text{ m}$  in three dimensions. We would like to point out that test cases are omitted if the package is not able to tackle them.

The results were obtained with the following set of regularization parameters: In case of `IPscatt` and `sparseScatt` we used the highest regularization parameter  $\alpha$ , that fulfills the discrepancy principle (20). Further, in the case of `IPscatt` we generally use  $\beta = \alpha \cdot 2 \cdot 10^{-8}$  as the second regularization parameter, because the ratio  $\alpha/\beta = 500/10^{-5}$  was derived empirically, cf. [Bürgel et al. 2017]. In addition, we enforce the real part of the contrast to be in  $[-1, 3]$  and the imaginary part to be in  $[0, 3]$  by using physical bounds in `IPscatt`. However, an exception of the  $\alpha$ - $\beta$ -ratio is made in `IPscatt` for the case of balanced penalty terms—i.e. sparsity penalty and total variation penalty have the same scale. Balanced penalty terms are recommended when reconstruction quality is paramount and increased computational cost is disregarded.

The reconstruction with `sparseScatt` turned out to be very sensitive to the choice of the step size of the thresholded, nonlinear Landweber scheme. If the value was chosen too small `sparseScatt` was very slow. If the value was chosen too big the reconstruction failed completely. After several experiments the value of  $10^{-4}$  was deemed best for the *Fresnel* case, cf. Fig. 5(c)/(g), and the value of 1 was deemed best for the *borehole* case, cf. Fig. 6(d)/(h).

In the case of `GLIDE` we took the same parameter values as were used in [Strehlow 2014, Sec. 5.5, Fig. 5.6].

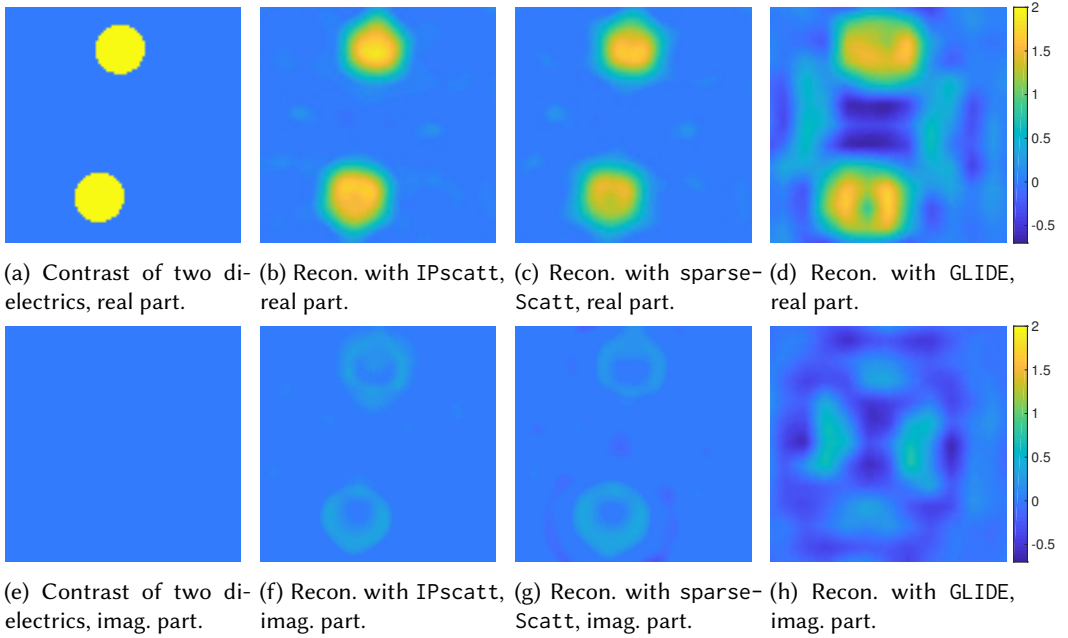


Fig. 5. Comparison of IPscatt with sparseScatt and GLIDE in two dimensions in the *Fresnel* case: exact contrast and reconstructions of two dielectrics from real-world data from Institute Fresnel with 6 GHz, real and imaginary part. The two dielectrics with a homogeneous contrast of  $q = 2 \pm 0.3$  have a radius of 15 mm and are positioned 45 mm from the origin. The reconstructions with IPscatt and sparseScatt were stopped by discrepancy principle. The reconstruction with GLIDE stopped because the maximum number of iterations was reached. The run times, relative discrepancies and relative errors were with IPscatt (b)/(f) 1.3 min, dis. 0.216, err. 0.542 after 6 iterations with  $\alpha = 10^6$ ,  $\beta = 0.02$ , with sparseScatt (c)/(g) 4.4 min, dis. 0.220, err. 0.552 after 50 iterations with  $\alpha = 114$  and with GLIDE (d)/(h) 0.8 min.

All computations were carried out on a workstation with an Intel(R) Core(TM) i7-3770 CPU with 3.40 GHz and 32 GByte RAM using MATLAB in version R2016b.

The contrast and the reconstructions relating the *Fresnel* case of the experimental set-up are shown in Fig. 5. As mentioned above GLIDE relies on the Born approximation and therefore is essentially comparable to IPscatt respectively sparseScatt with only one outer loop. However, as can be seen in Fig. 5(d)/(h) the resulting reconstruction is reasonable. A better reconstruction is obtained with sparseScatt with a significantly higher computational cost, see Fig. 5(c)/(g). However, one notices that both reconstructions contain regions where the imaginary part of the contrast is negative, i.e. the obtained reconstructions are physically not sensible. Finally, since the reconstruction approach of IPscatt is based on physical constraints, it is able to avoid these artifacts, see Fig. 5(b)/(f). At the same time it has only slightly higher computational cost than GLIDE.

Next, the contrast and the reconstructions relating the *borehole* case are presented in Fig. 6. The result of IPscatt was accurate and fast again, see Fig. 6(c)/(g). As in the previous example, the reconstruction obtained by sparseScatt is reasonable as determined by visual inspection, see Fig. 6(d)/(h). It is not surprising that the same physical artifacts as were discussed in the *Fresnel* case are also encountered here. Further, we observe some artifacts around the rotated thin line. Moreover, sparseScatt was much slower than IPscatt. In addition, we reconstructed the contrast with



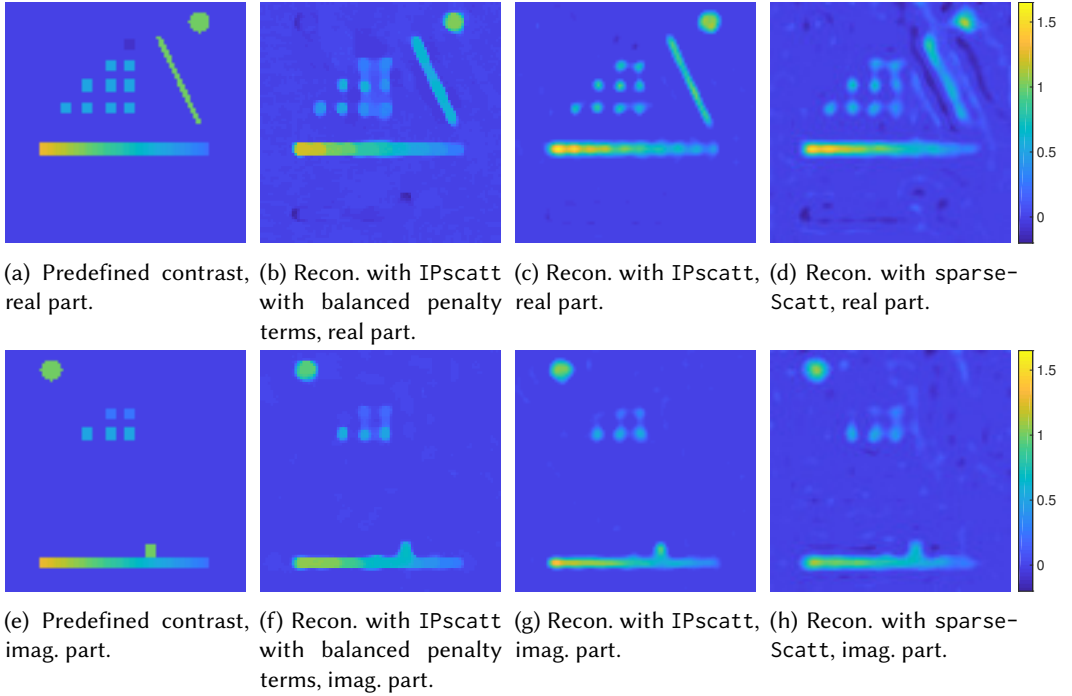


Fig. 6. Comparison of IPscatt (with and without balanced penalty terms) with sparseScatt in two dimensions in the *borehole* case: predefined contrast and reconstructions in real and imaginary part from simulated data with 1% noise level. The reconstructions with IPscatt and sparseScatt were stopped by discrepancy principle. The run times, relative discrepancies and relative errors were with IPscatt using balanced penalty terms (b)/(f) 12.4 h, dis. 0.026, err. 0.333 after 64 iterations (with  $5 \cdot 10^5$  inner iterations in the last one) with  $\alpha = 2.04 \cdot 10^{-4}$ ,  $\beta = 6 \cdot 10^{-7}$ , with IPscatt (c)/(g) 16.5 min, dis. 0.025, err. 0.337 after 62 iterations with  $\alpha = 310$ ,  $\beta = 6.2 \cdot 10^{-6}$  and with sparseScatt (d)/(h) 5.1 h, dis. 0.015, err. 0.455 after 2319 iterations with  $\alpha = 10^{-4}$ .

IPscatt with the above mentioned balanced penalty terms, see Fig. 6(b)/(f). The thick horizontal rectangle is excellently recovered as well as is the gradual contrast ramp. However, the thickness of the thin diagonal line is overestimated by the reconstruction algorithm.

Finally, the contrast and the reconstruction relating the *sphere* case of the experimental set-ups are shown in Fig. 7. As neither sparseScatt nor GLIDE support reconstructions for scattering in three dimensions only the reconstruction obtained by IPscatt is shown. As can be seen it delivers a precise reconstruction result in a reasonable time.

*Discussion.* All three software packages have in common routines of the *Data Readers* group to deal with real-world data from Institute Fresnel and routines of the *Scattering Simulation* group. In the latter case, the only difference concerns the dimension: all can deal with 2D but only IPscatt with 3D. Therefore we focus on the groups *Experimental Set-Up* and *Contrast Reconstruction* in the discussion.

Out of the box the software package GLIDE is restricted to two-dimensional scattering problems and transmitter-receiver geometries on circles. GLIDE has these properties in common with sparseScatt. As the only package, amongst the three considered, GLIDE is restricted to small wave numbers because it solves the linear inverse medium problem instead of the nonlinear one. Consequently, in the case of high wave numbers GLIDE cannot compete with sparseScatt and IPscatt with

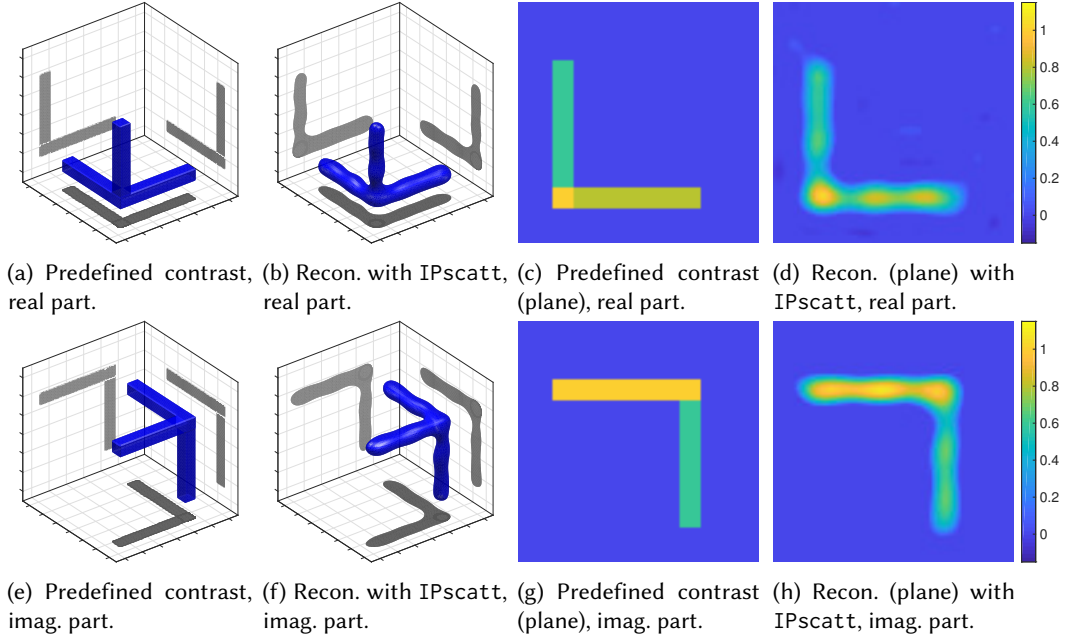


Fig. 7. *Sphere* case: reconstruction of two tripods in real and imaginary part with IPscatt from simulated data with 1% noise level. The arcs of the tripods have the contrast values 1.0, 0.8, 0.6 and  $1.0i$ ,  $0.8i$ ,  $0.6i$ . The contrast on a sectional plane through the scatterer is shown in the second direction in the case of the real part and the first direction in the case of the imaginary part. Parameters for reconstruction were  $\alpha = 1000$ ,  $\beta = 2 \cdot 10^{-5}$ . The reconstruction was stopped by the discrepancy principle after 15 iterations. The run time was 6.01 h, relative discrepancy 0.012 and relative error 0.464.

regard to reconstruction quality. On the other hand, GLIDE outcompetes the compared packages with the low computational effort. Altogether, GLIDE is recommended only if the run time is the most important factor.

The package `sparseScatt` is also restricted to two-dimensional scattering problems and to transmitter-receiver geometries on circles. Further, among the three compared packages `sparseScatt` was consistently the computationally most expensive one. However, `sparseScatt` can deal with the nonlinear inverse medium problem and therefore delivers a better reconstruction than GLIDE but stays behind IPscatt.

The only disadvantage of IPscatt in comparison to GLIDE and `sparseScatt` is the slightly higher computational effort in comparison to GLIDE. Altogether one can summarize that IPscatt provides a better usability, reconstruction quality and run time properties than GLIDE or `sparseScatt`.

## 5 SUMMARY AND OUTLOOK

We have discussed the main features and application cases of IPscatt. We have also compared it to other existing software packages dealing with the inverse medium problem in time-independent scattering. The comparisons were carried out for synthetic as well as real-world data.

We are confident that the modular and flexible design of IPscatt facilitates its use in a wide range of applications. For example, the ability to define arbitrary transmitter and receiver geometries is interesting for users interested in the simulation of scattering with extremely few transmitters and

receivers. Together with IPscatt's sophisticated reconstruction algorithm it allows to study the limit cases of reconstructability in the inverse medium problem.

However, several open questions remain. For example, it is well-known that the quality of the reconstruction is dependent on a suitable choice of the involved regularization parameters. Therefore a subject of ongoing research is a heuristic algorithm for an automatic, data-driven parameter choice.

In addition, there are still two interesting open questions regarding the scattering simulation's and the reconstruction scheme's theory. The first question is about the convergence of the collocation method. In the case of smooth contrasts it was proven in [Vainikko 2000]. However, in the case considered here, i.e. piecewise smooth contrasts, the convergence was usually given in our numerical experiments but its proof remains elusive. The second question is about the convergence of the underlying reconstruction scheme. Some of its aspects like the usage of the primal-dual algorithm are justified by [Chambolle and Pock 2011; Pock et al. 2009] but its connection to the properties of the outer iterations is yet to be entirely understood. However, as above although the proof is still a matter of current research, the proposed reconstruction scheme turned out to be reliable in comprehensive numerical experiments in two and three dimensions, in particular, in the case of real-world data in two dimensions.

## ACKNOWLEDGMENTS

The research of all authors was funded by the Deutsche Forschungsgemeinschaft (DFG, German Research Foundation) under grants Ka 3954/1-1 and Le 2499/2-1.

## REFERENCES

- Milton Abramowitz and Irene A. Stegun. 1965. *Handbook of mathematical functions* (unabridged and unaltered republication of the 1964 ed.). Dover books on intermediate and advanced mathematics, Vol. 44. Dover Publications, New York.
- Amir Beck and Marc Teboulle. 2009. A Fast Iterative Shrinkage-Thresholding Algorithm for Linear Inverse Problems. *SIAM Journal on Imaging Sciences* 2, 1 (2009), 183–202. <https://doi.org/10.1137/080716542>
- Kamal Belkebir and Marc Saillard. 2001. Special section on testing inversion algorithms against experimental data. *Inverse Problems* 17, 6 (2001), 1565–1571. <https://doi.org/10.1088/0266-5611/17/6/301>
- Carlos Borges, Adrianna Gillman, and Leslie Greengard. 2017. High Resolution Inverse Scattering in Two Dimensions Using Recursive Linearization. *SIAM Journal on Imaging Sciences* 10, 2 (2017), 641–664. <https://doi.org/10.1137/16M1093562>
- Max Born. 1926. Quantenmechanik der Stoßvorgänge. *Zeitschrift für Physik* 38, 11 (1926), 803–827. <https://doi.org/10.1007/BF01397184>
- Florian Bürgel, Kamil S. Kazimierski, and Armin Lechleiter. 2017. A sparsity regularization and total variation based computational framework for the inverse medium problem in scattering. *J. Comput. Phys.* 339 (2017), 1–30. <https://doi.org/10.1016/j.jcp.2017.03.011>
- Antonin Chambolle and Thomas Pock. 2011. A First-Order Primal-Dual Algorithm for Convex Problems with Applications to Imaging. *Journal of Mathematical Imaging and Vision* 40, 1 (2011), 120–145. <https://doi.org/10.1007/s10851-010-0251-1>
- Tony F. Chan and Jianhong (Jackie) Shen. 2005. *Image Processing and Analysis*. Society for Industrial and Applied Mathematics, Philadelphia. <https://doi.org/10.1137/1.9780898717877>
- David Colton and Rainer Kress. 2013. *Inverse Acoustic and Electromagnetic Scattering Theory*. Springer, New York. <https://doi.org/10.1007/978-1-4614-4942-3>
- Heinz W. Engl, Martin Hanke, and Andreas Neubauer. 1996. *Regularization of inverse problems*. Kluwer Academic Publishers, Dordrecht, Netherlands.
- Álvaro González. 2010. Measurement of Areas on a Sphere Using Fibonacci and Latitude–Longitude Lattices. *Mathematical Geosciences* 42, 1 (2010), 49. <https://doi.org/10.1007/s11004-009-9257-x>
- C. Tim Kelley. 1995. *Iterative Methods for Linear and Nonlinear Equations*. Society for Industrial and Applied Mathematics. <https://doi.org/10.1137/1.9781611970944>
- C. Tim Kelley. 2002. Iterative Methods for Linear and Nonlinear Equations. Companion Software. <https://de.mathworks.com/matlabcentral/fileexchange/2198-iterative-methods-for-linear-and-nonlinear-equations/content/kelley/gmres.m>. Accessed: March 2017.
- Armin Lechleiter, Kamil S. Kazimierski, and Mirza Karamahmedović. 2013. Tikhonov regularization in  $L^p$  applied to inverse medium scattering. *Inverse Problems* 29, 7 (2013), 075003. <https://doi.org/10.1088/0266-5611/29/7/075003>

- Armin Lechleiter and Marcel Rennoch. 2017. Non-linear Tikhonov Regularization in Banach Spaces for Inverse Scattering from Anisotropic Penetrable Media. *Inverse Problems and Imaging* 11, 1 (2017), 151–176. <https://doi.org/10.3934/ipi.2017008>
- Thomas Pock, Daniel Cremers, Horst Bischof, and Antonin Chambolle. 2009. An algorithm for minimizing the piecewise smooth Mumford-Shah functional. In *IEEE International Conference on Computer Vision (ICCV)*. 1133–1140. <https://doi.org/10.1109/ICCV.2009.5459348>
- Marcel Rennoch. 2017. *Regularization Methods in Banach Spaces Applied to Inverse Medium Scattering Problems*. Ph.D. Dissertation. Universität Bremen. Retrieved from <https://nbn-resolving.de/urn:nbn:de:gbv:46-00105983-18>.
- Andreas Rieder. 2001. On convergence rates of inexact Newton regularizations. *Numer. Math.* 88, 2 (2001), 347–365. <https://doi.org/10.1007/PL00005448>
- Robin Strehlow. 2014. *Regularization of the inverse medium problem: on nonstandard methods for sparse reconstruction*. Ph.D. Dissertation. Universität Bremen. Retrieved from <https://nbn-resolving.de/urn:nbn:de:gbv:46-00104187-19>.
- Gennadi Vainikko. 2000. Fast Solvers of the Lippmann-Schwinger Equation. In *Direct and Inverse Problems of Mathematical Physics*, Robert P. Gilbert, Joji Kajiwara, and Yongzhi S. Xu (Eds.). Springer, Boston, 423–440. [https://doi.org/10.1007/978-1-4757-3214-6\\_25](https://doi.org/10.1007/978-1-4757-3214-6_25)
- Lexing Ying. 2015. Sparsifying Preconditioner for the Lippmann-Schwinger Equation. *Multiscale Modeling & Simulation* 13, 2 (2015), 644–660. <https://doi.org/10.1137/140985147>

Received October 2017; revised August 2018; revised April 2019; accepted April 2019